THE JOURNAL OF PHYSICAL CHEMISTRY C

Article

pubs.acs.org/JPCC

Adhesive Properties of Gecko-Inspired Mimetic via Micropatterned Carbon Nanotube Forests

Bingan Chen,[†] Pola Goldberg Oppenheimer,*[,†] Tamaryn A.V. Shean,[‡,§] C. Tobias Wirth,[†,∥] Stephan Hofmann,[†] and John Robertson[†]

[†]Department of Engineering, University of Cambridge, JJ Thomson Avenue, Cambridge, CB3 0FA, U.K.

[‡]Department of Engineering, University of Cambridge, Trumpington Street, Cambridge, CB2 1PZ, U.K.

ABSTRACT: The adhesive properties of the gecko foot have inspired designs of advanced micropatterned surfaces with increased contact areas. We have fabricated micropatterned pillars of vertically aligned carbon nanotube forests with a range of pillar diameters, heights, and spacings (or pitch). We used nanoindentation to measure their elastic and orthogonal adhesion properties and derive their scaling behavior. The patterning of nanotube forests into pillar arrays allows a reduction of the effective modulus from 10 to 15 MPa to 0.1−1 MPa which is useful for developing maximum conformal adhesion.

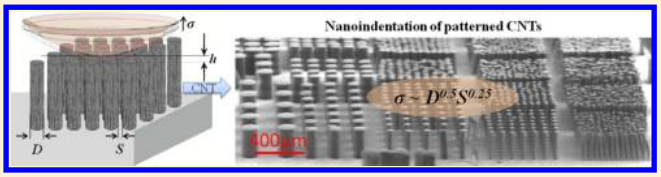

1. INTRODUCTION

The unique adhesive properties of fine hair multilevel conformal systems commonly found in lizards (e.g., geckos, anoles) and insects (e.g., stick insects, spiders) are a topic of extensive research.[1−18] Their ability to reversibly adhere to virtually any surface and orientation has inspired many potential applications, ranging from bioinspired artificial analogues[3−5] to flexible adhesive tapes.[6] The adhesion arises from weak van der Waals forces between the foot and the contacted surface, but the adhesion is increased to large values by the principle of contact splitting.[1,7] Splitting one contact into N contact for a given area will increase the adhesion by $N^{1/2}$.

The biomimetic adhesive surfaces can be fabricated in two ways, either *bottom-up* or *top-down*.[6,10−17] The top-down approach consists of fabricating lithographically defined polymer hairs,[10−14] while the bottom-up approach can consist of growing forests of vertically aligned carbon nanotubes (CNTs).[6,16−18] However, it has still been difficult to achieve adhesive performances matching those found in nature.[19−22] We have yet to be able to fabricate an optimal hierarchical fiber structure which provides a high adhesive force combined with superior adaptation and reversible adhesion to dry rough surfaces.

CNTs are well-known for their exceptional mechanical properties and are one of the most promising materials to use for gecko-inspired dry adhesives.[16,19] CNTs have a Young's modulus of about 1 TPa, and we can vary the diameter of a nanotube from 1 to 100 nm and grow them up to 5 mm high. This combination of high aspect ratio, high rigidity, and controllable height allows us to vary the strength, stiffness, and flexibility to optimize the adhesion force.[16,18,23] We can grow vertically aligned CNT (VACNT) forests on surfaces by catalytic chemical vapor deposition (CVD).[15−18] We can control the CNT diameter by the thickness of catalyst used, and we can pattern the catalyst to create pillars of the VACNT forests.

Qu et al.[24] showed that single-walled carbon nanotube forests (SWCNTs) had a high shear adhesion strength. The adhesive performance was further improved by using aligned multiwalled carbon nanotube (MWCNT) arrays with entangled tip segments.[16] Ge et al.[6] showed that micropatterned CNT arrays increased the shear adhesion compared to the nonpatterned VACNTs since they prevented crack propagation during the detachment. This shows that the contact splitting principle also applies to VACNT arrays. Patterned surfaces were shown to increase the adhesion to surfaces of varying roughness.[20,25−29]

Nevertheless, the existing literature has been largely aimed at maximizing adhesive performance. There has been less measurement of the basic elastic and adhesive properties as a function of surface architecture. Therefore, in this work we fabricate and systematically investigate adhesive properties of patterned VACNTs in pillar geometries with a broad range of pattern sizes, aspect ratios, and spacings. This is accomplished by using the nanoindentation technique, which is a well-known approach to measure hardness of materials and structured substrates.[30,31] Although commonly used for studying the mechanical properties of materials, nanoindentation has been rarely employed for measuring the adhesive properties of VACNT arrays. Although atomic force microscopy (AFM) has been used for small-scale indentation testing,[32] the direct application of loads in nanoindentation is advantageous compared to the indirect loading with an AFM cantilever, because of the extensive calibration of the cantilever that is needed. Also nanoindentation enables a greater degree of control and better analysis of the snap-on and pull-off forces at the contact point during the approach and retract of the probe.[33]

Received: May 14, 2012
Revised: August 2, 2012
Published: August 24, 2012

   dx.doi.org/10.1021/jp304650s | *J. Phys. Chem. C* 2012, 116, 20047−20053

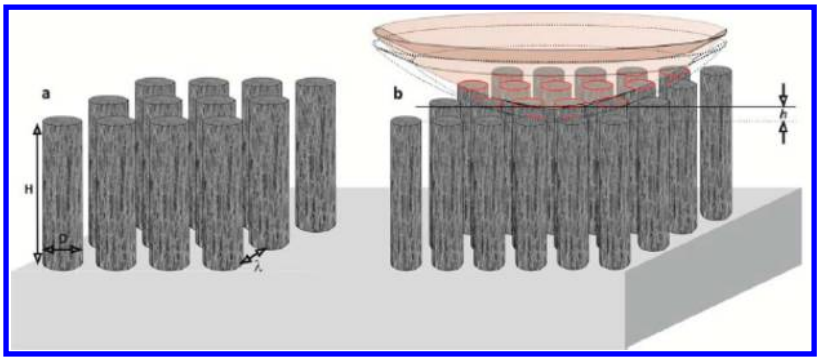

Figure 1. Schematics of the patterned VACNT pillar arrays (a) with diameter, *D*, height, *H*, and pitch distances between the structures, λ and (b) subjected to the nanoindentation test. The actual contact area (outlined as red cylindrical tops) measured via nanoindentation varies with preload and is calculated based on the indentation depth, *h*.

In nondestructive nanoindentation testing, a small-scale surface probe of specified geometry is brought into and out of contact with a material surface, using a constant loading and unloading rate. The load, displacement, and time are recorded over the test, and they are analyzed using analytical techniques appropriate for the material.[34,35] Testing VACNTs using nanoindentation is advantageous as we can test their properties on the same length scale as the forests themselves. We can alter the probed length scale merely by varying the tip size or maximum penetration depth. This allows characterization of either a single VACNT pillar or a patterned array of VACNT pillars with variations in *pitch* (λ) between the arrays (Figure 1a). Interestingly, λ plays an important role in the adhesion strength of VACNT pillars, highlighting a key parameter previously overlooked in designing CNT-based gecko-like structures.

2. EXPERIMENTAL SECTION

CNT Growth. Polished Si(100) (5 × 5 mm^2) wafers are used as substrates, covered with 200 nm thermally grown SiO_2. Al_2O_3 support layers and Fe catalyst layers are sputter deposited from Al_2O_3 (99.99% purity) and Fe (99.99% purity) targets, respectively. Electron-beam lithography is used to pattern the Al_2O_3/Fe stacks for subsequent CVD growth of VACNT pillar arrays. Arrays are patterned with spacings from 3 to 150 μm by lift-off. Nanotube CVD follows the process previously described by Zhong and Wirth.[36,37] Samples are exposed to an atmosphere of 500 sccm H_2 and heated to 700 °C in 5 min for the pretreatment step. The total pressure is kept at 15 mbar. The CNTs are grown in a gas flow of 460:40 sccm H_2:C_2H_2 for 5 min. Upon completion of growth, the substrate is cooled to room temperature under 500 sccm H_2. The growth time is varied to control the VACNT heights ranging from 170 to 230 μm. The individual pillar diameters range between 15 and 150 μm.

Adhesion Measurements. Adhesion tests were performed using a UBI 1 (TI-700, Hysitron Inc.) with a sapphire spherical tip (radius of 400 μm). A displacement controlled trapezoidal loading profile with 10 s load, hold, and unload times each were used.[30,31] The measured adhesive forces were normalized by the actual contact area between the pillar surfaces and the indenter. The actual contact area was calculated using the law of cosines and an area of πr^2 (Figure 1b), assuming the apparent contact area is the ratio of the cross-sectional area of the indenter to the maximum displacement distance. The maximum displacement is set to 4 μm to obtain a contact diameter of between 98 and 112 μm.

The effective Young's Modulus of the CNT pillars was calculated using the Oliver–Pharr (OP) model[38] from the elastic unload stiffness, which is the initial slope of the experimental unloading curve. During tip unloading, the adhesion was measured as the maximum pull-off force required to remove the tip from the material surface.

3. RESULTS AND DISCUSSION

Figure 2a,b shows representative arrays of patterned VACNT pillars with various pillar diameters (15–150 μm) and

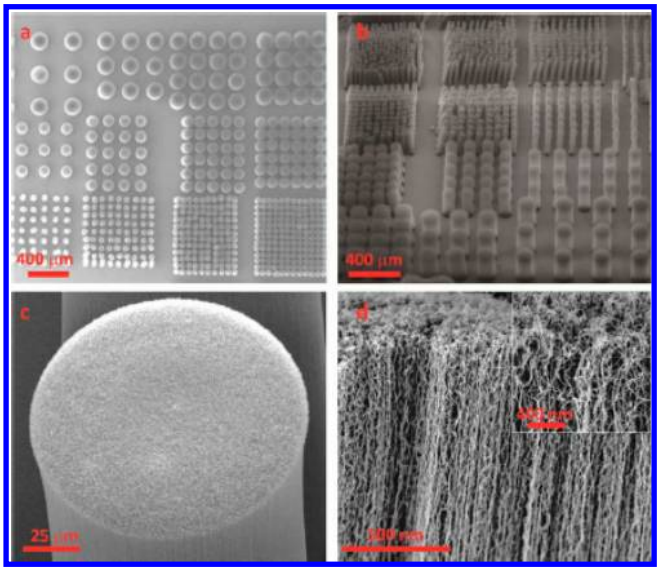

Figure 2. Microfabricated vertically aligned carbon nanotube setae and spatulas. SEM images of top view (a) and three-dimensional view (b) of VACNTs pillars with different pillar widths (15–150 μm) and pillar spacing distances. The minimum interpillar spacing is 3 μm. An individual 100 μm diameter pillar (c) comprised of well-aligned multiwall carbon nanotubes (d) with curly entangled nanotubes ends (d, inset).

interpillar spacing (3–150 μm). These arrays were batch-fabricated on a single substrate with a square symmetry. These values are similar to those found in gecko species, which act to prevent the undesirable lateral collapse of high aspect ratio patterns, which can be detrimental to adhesion.[6] An individual 100 μm pillar (Figure 2c) of VACNTs is clearly seen in the cross-sectional SEM image in Figure 2d. The multiwalled nanotubes have an average diameter of 10 nm and ~8 walls.

A characteristic nanoindentation adhesion test is comprised of pressing the tip into the patterned sample, followed by unloading it at a constant rate and finally obtaining a distinctive (and often abrupt) pull-off force representing the adhering surfaces. Figure 3 shows a typical load versus displacement curve obtained during the nanoindentation with the loading, unloading, and pull-off adhesion forces.

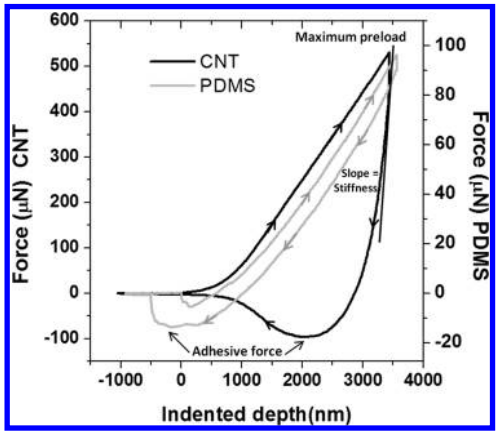

Figure 3. Typical load vs displacement curves. Considerable differences are seen in the nanoindentation curves for VACNTs (black line) and a standard polymer, i.e., polydimethyl-siloxane (PDMS) (gray line), with similar dimensions.

Conventional analysis of nanoindentation was based on the Hertz contact model, applicable for ideal materials experiencing infinitesimal deformation at the loading process. This is a hard contact model which ignores the adhesive interaction. The OP model on the other hand includes both the elastic and the adhesive force. The compressive parts of the force−distance curves in our study were analyzed using the OP model, while meeting the conditions of a rigid-parabolic indenter and nonlinear unloading characteristics of the load−displacement curve (Figure 3), yielding the effective Young's modulus.[38]

The initial unloading stiffness, S, obtained from the slope of the unloading curve (Figure 3) is given by

$$S = \frac{dP}{dh} = \frac{2}{\sqrt{\pi}} E_r \sqrt{A} \tag{1}$$

where E_r is the effective modulus of the surface and A is the cross-sectional contact area of the indenter at maximum displacement. Given that the tip's stiffness is considerably larger than the sample's, the effective Young's modulus in OP theory[37] is then

$$E_r = \frac{E}{(1 - \nu^2)} \tag{2}$$

where E is the Young's Modulus and υ is Poisson's ratio. The Poisson's ratio can be taken as zero for VACNT forests.[39]

The Young's modulus of our uniform VACNT forest is 15 MPa, which compares to the Young's modulus of a single CNT of about 1 TPa. The forest has an area fill factor, f, of about 5%. If the forest is modeled as a cellular solid,[40] the modulus scales as f^2

$$E = E_0 c f^2 \tag{3}$$

This would need quite a rather low prefactor $c = 0.0067$ to fit the data.

The effective Young's modulus for the patterned VACNT forests as a function of pillar aspect ratio and pillar spacing is shown in Figure 4. An increase in the pillar aspect ratio at constant diameter decreases E_r, and the effective modulus decreases with decreasing pillar diameter (Figure 4a). These results are consistent with previous reports by Glassmaker et al.[12] for polymer pillars, who show that the Young's modulus decreases with increasing aspect ratio due to fibril bending, making the effective compliance more sensitive to the aspect ratio.

Figure 5 plots the pillar's reduced Young's modulus vs fill factor times pillar diameter, for various pillar diameters. This plot shows that E varies as $E \sim E_0(FD)$. Here F is the fill factor of pillars, $\pi D^2/4\lambda^2$; D is the pillar diameter; S is the spacing; and the spacing $\lambda = D + S$. We see that increasing the pitch can be used to reduce the Young's modulus from the unpatterned value of 15 MPa to any chosen value. It is known that softer effective moduli of the order of 0.1−1 MPa are useful for adhesives as they allow a surface to conform to any local roughness of the contacted surface, thereby increasing contact area with the minimum increase in elastic energy. This is related to the Dahlquist criterion.[21,45]

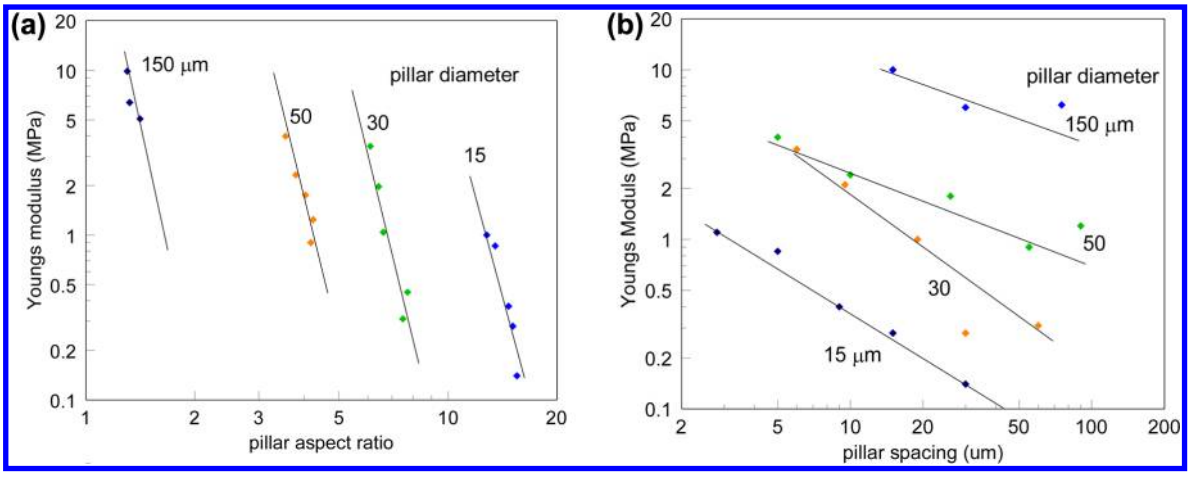

Figure 4. Effective Young's modulus as a function of (a) pillar aspect ratio and (b) pillar spacing between the nanotube pillars of various diameters. Higher values of E_r are obtained for larger pillar diameter, with decreasing trends for increasing aspect ratio (a) and the pillar spacing size (b).

dx.doi.org/10.1021/jp304650s | J. Phys. Chem. C 2012, 116, 20047−20053

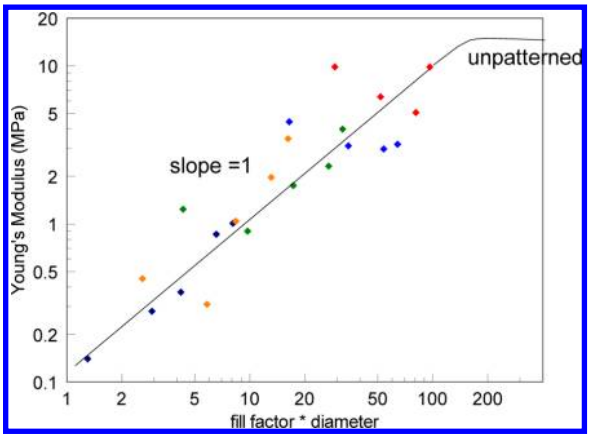

Figure 5. Variation of Young's modulus with fill factor times diameter, for pillars of different diameter, showing a linear relationship.

Returning to Figure 3, the indentation curves for the VACNT pillars show a distinctive difference from those found for conventional polymers such as polydimethyl-siloxane (PDMS). First, there is a difference in the initial preloading point, where the jump to contact plays an important role. Jump to contact describes the sudden increase in forces which draws the contacted material toward the approaching tip as it comes within range of the van der Waals forces. This characteristic is more clearly seen for the polymer surface than CNT surfaces during preloading. During preloading, the force constantly increases until the indenter reaches a certain depth, h, where the maximum preload force is obtained. Figure 3 clearly shows that a larger preload is required to achieve the same indentation depth for VACNT pillars compared to polymers. According to the Oliver–Pharr model,[39] the material's Young's modulus can be extracted from the slope of the early unloading. A significant approach-retraction hysteresis is observed for the VACNT arrays compared to patterned polymer surfaces (Figure 3). This effect indicates that the VACNT arrays exhibit a more plastic deformation and are considerably stiffer than the conventional (predominantly viscoelastic) polymer response.

There is a large difference in the recovery and the pull-off point between the VACNTs and PDMS samples. The pull-off force is obtained at a positive value of indented depth (Figure 3, black line), and the force gradually recovers to zero. This is due to the plastic deformation of the VACNT arrays during loading. For the more elastic and adhesive PDMS, the unloading curve closely tracks the loading curve, while the pull-off force is obtained at a negative indented depth (Figure 3, gray line) and the load suddenly jumps to zero after the pull-off point.

Figure 6 shows the measured pull-off strength for preloads on VACNT pillars of different diameter. As the actual contact area during the nanoindentation measurement varies for each preload, it directly influences the pull-off force. Thus, the pull-off strength is used as a more representative value for adhesion performance comparison. The pull-off strength is calculated by

$$\sigma = \frac{F}{A_{\text{actual}}} \tag{5}$$

where σ is the pull-off strength; F is the pull-off force; and A_{actual} is the actual contact area between the tip and the CNT pillar surface (Figure 1b) at a certain nanoindentation depth (see Experimental Section for details). We use this approach rather than estimating a work of adhesion within the context of a Johnson–Kendal–Roberts (JKR) model.[41]

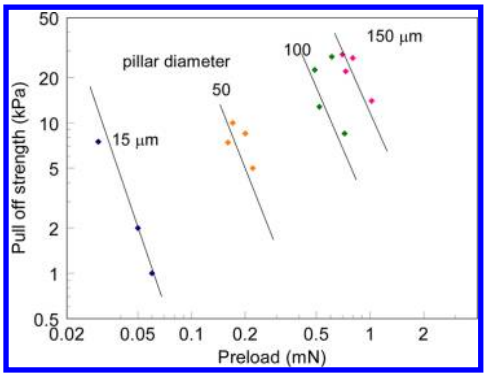

Figure 6. Variation of the pull-off strength as a function of preload force for different VACNT pillar diameters. Lines are a guide to the eye.

While the adhesion strength decreases with increasing preload at constant pillar diameter, in agreement with the trend seen for patterned polymer surfaces,[13] a higher pull-off strength is clearly seen for VACNT pillars with larger diameter. This is in contrast to patterned polymer surfaces, where decreasing pillar radii show higher adhesion forces.[13] According to the contact splitting principle,[1,25] the polymer-based structures require smaller diameter structures to support larger adhesive forces. Larger radii micrometer scale setae in addition to the nanometer CNTs are needed for higher adhesion forces.[6]

VACNT pillars of greater heights at a constant pillar diameter show an increased pull-off strength with increasing aspect ratio (Figure 7a). This is similar to the increased adhesion at larger aspect ratios found for polymer patterns.[13,28,42] This is explained by the fact that at the pull-off point where adhesive fails the strain energy stored in the stretched tubes is dissipated, contributing to the total work of adhesion. In longer tubes, the stored elastic energy just before pull-off is greater than in the shorter tubes with the same diameter. Therefore, more energy is lost during the detachment of higher aspect ratio VACNT pillars.[20] The high aspect ratio VACNT pillars provide adaptability to rough surfaces due to the long fibrillar elements and an easy bending with minimum of elastic energy storage. Thus, a higher aspect ratio not only enhances the adhesion force but also increases flexibility, allowing a conformation to surfaces of arbitrary roughness.[43]

The spacing between the adjacent VACNTs pillars is also found to affect adhesion strength (Figure 7b). Plotting pull-off strength σ against combinations of diameter D and spacing S, we find that σ varies as

$$\sigma \sim D^{0.5} S^{0.25} \tag{6}$$

as seen in Figure 7c. There is considerable data in the literature about adhesion of patterned polymer arrays as a function of structural parameters (e.g., diameter, aspect ratio, shape, etc.).[13,20,44,45] However, there is much less data for CNT-based structures and in particular no data for the variation of pull-off strength with spacing. Figure 7b shows that an increase in the spacing causes an increase in the adhesion strength. It should be noticed that the pillar spacing is smaller than pillar height here. Too small a spacing typically causes a lateral collapse of the pillars during attachment.[10−12] This causes a loss of contact area between the VACNT pillars and the tip, consequently reducing the adhesion strength. On the other hand, a larger spacing between the pillars prevents the neighboring pillar interactions. It is found that the spacing is

dx.doi.org/10.1021/jp304650s | J. Phys. Chem. C 2012, 116, 20047−20053

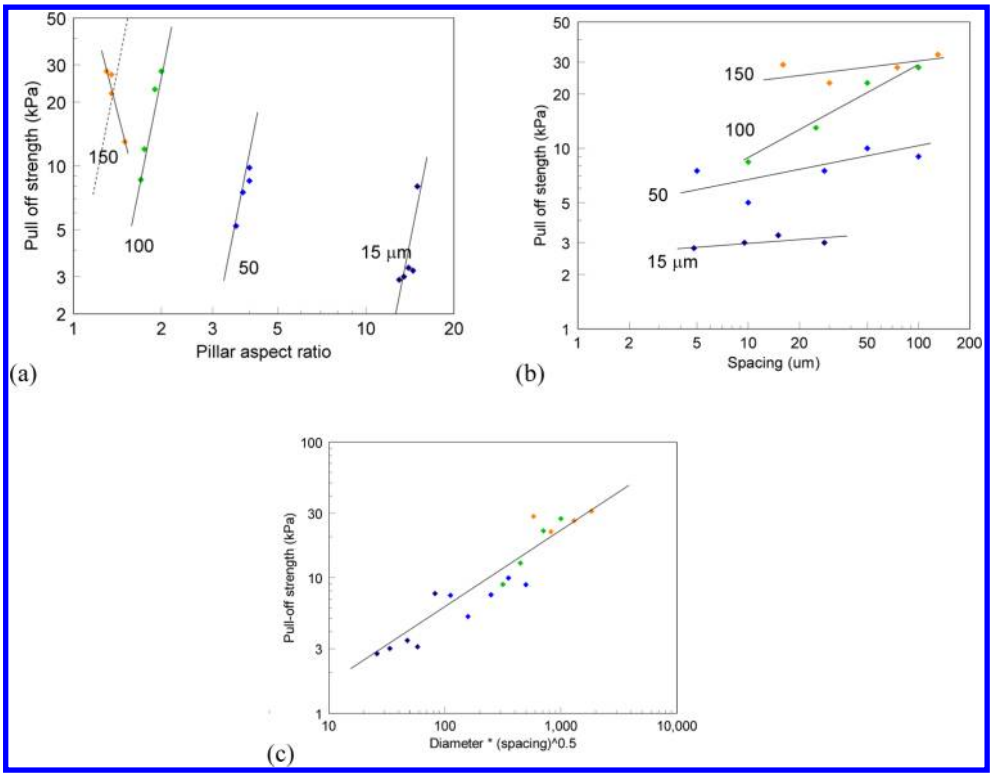

Figure 7. Pull-off strength increases with pillar diameter. For a constant diameter, the pull-off strength increases for both the (a) aspect ratio and (b) the pillar spacing. Lines are a guide to the eye. (c) Scaling relationship between pull-off strength and pillar diameter*(spacing)$^{0.5}$ giving a slope of 0.55.

Table 1. Comparison of Adhesive Strength Measured by Indentation for Various Synthetic Materials

material	Young's Modulus (MPa)	probe radius (cm)	preload (mN)	pull-off force (mN)	pull-off strength (kPa)	adhesion coefficient
organorods[30]	-	0.3	12	0.45	-	0.04
polyurethane[50]	0.62	0.005	0.1	0.012	-	0.12
PDMS[51]	1.9	0.25	0.5	0.07	2.15	0.14
polypropylene[52]	-	5	2	<0.05	-	0.4
PDMS[13]	1.5	0.25	2	1.1	10	0.5
polyurethane[27]	3	1.2	256	600	37	2.3
VACNT pillars	0.1−10	0.04	0.8	0.25	26	0.3

a useful factor for controlling adhesion force and the design of artificial adhesive surfaces.

It can be seen from Figures 4a and 7a that the larger pattern diameter leads to higher adhesion strength and effective Young's modulus. Considering that pillars with larger diameters exhibit larger actual contact area during a nanoindentation test. Pillar spacing is an additional important factor found to influence the effective Young's Modulus. Larger spacing results in lower pillar packing density, subsequently reducing the indentation area, while the nanoindenter contacts fewer pillars. Therefore, the effective Young's modulus decreases with the increasing pillar spacing (Figure 7b).

A successful mimicking of attachment pads with strong adhesive forces similar to the gecko remains a highly desirable and broadly explored goal.[19,20,45−47] While structures on the micrometer scale with various geometries are shown to be sufficient for good adhesion to support larger adhesive forces, contact splitting into finer elements is required. Carbon nanotubes patterned into micrometer structures are very promising candidates for this task as they include micrometer-size structures that mimic setae along with nanometer-size structures that are analogues of spatulas. Table 1 summarizes the most common synthetic analogues to mimic climbing animals' performance.

The unique properties of the gecko foot arise from a combination of sufficient softness (effective Young's Modulus <100 kPa) to conform to any surface roughness along with high mechanical stability (with individual Young's Modulus of 1−3 GPa).[48] VACNT pillars with large aspect ratios (Figure 4a-b) exhibit effective Young's Modulus values similar to the gecko setaes. Thus, taking into account the large Young's Modulus of a single nanotube (~1000 GPa[49]), patterned CNT arrays are promising candidates for gecko-foot-mimetic materials.

Since the pull-off force is directly related to the preload force, it is more meaningful to compare the adhesion coefficient, defined as the ratio between the pull-off force and the preload. The higher the adhesion coefficient, the smaller the contact force needed to engage the adhesive. The VACNT pillars in our study are found to have an adhesion coefficient of 0.3 with a normal adhesion force of 26 kPa, while for a natural gecko foot hair the normal pull-off strength is found to be around 10 kPa.[2] The adhesive characteristics, measured by nanoindentation, are in agreement with the CNT adhesion measurements performed on the macroscale by Qu et al.,[16] which found the normal

dx.doi.org/10.1021/jp304650s | J. Phys. Chem. C 2012, 116, 20047−20053

adhesion of the CNTs to be 20 kPa. Nevertheless, it is important to point out that further studies of the pull-off force in the shear direction (expected to be stronger than those in the normal direction) are essential to mimic the closer-to-nature gecko movement which requires easy lifting-off and strong shear binding-on.

4. CONCLUSIONS

We used nanoindentation to test the orthogonal adhesive properties of pillar arrays of vertically aligned carbon nanotubes with varied dimensions. Their adhesive properties were found to depend strongly on the pillar diameter, aspect ratio, and pillar spacing. Pillars with higher aspect ratio resulted in larger adhesion and also increased the adaptability to rough surfaces due to the smaller effective Young's modulus. Increased spacing also allowed stronger adhesive forces and prevents clustering interactions between the neighbor pillars while lowering the effective Young's Modulus. Therefore, by altering these parameters, VACNT pillar substrates can be tuned to provide a variety of advanced adhesive-based applications.

Additionally, the VACNT structures display good adhesive but nonsticky properties, in contrast to the previously demonstrated tapes or polymer-based materials such as PDMS used for synthetic adhesive mimics. This nonsticky characteristic enables improved ability to climb, move, and peel the feet or the structure off the surface. The patterned VACNT surfaces are therefore a useful system from which to design gecko-foot-mimetic adhesives.

AUTHOR INFORMATION

Corresponding Author

*Tel. +44-1223-748317. E-mail: pg333@cam.ac.uk.

Present Addresses

[§]National Physical Laboratory, Teddington, London TW11 0LW, U.K.

[∥]Philips Electronics, Amstelplein, Amsterdam 1096C, Netherlands.

Notes

The authors declare no competing financial interest.

ACKNOWLEDGMENTS

The authors acknowledge funding from the EC project Technotubes. Michelle L. Oyen is kindly acknowledged for her inputs.

REFERENCES

(1) Arzt, E.; Gorb, S.; Spolenak, R. *Proc. Natl. Acad. Sci.* **2003**, *100*, 10603.

(2) Autumn, K.; Liang, Y. A.; Hsieh, S. T.; Zesch, W.; Chan, W. P.; Kenny, T. W.; Fearing, R.; Full, R. J. *Nature* **2000**, *405*, 681.

(3) Mahdavi, A.; Ferreira, L.; Sundback, C.; Nichol, J. W.; Chan, E. P.; Carter, D. J. D.; Bettinger, C. J.; Patanavanich, S.; Chignozha, L.; Ben-Joseph, E.; Galakatos, A.; Pryor, H.; Pomerantseva, I.; Masiakos, P. T.; Faquin, W.; Zumbuehl, A.; Hong, S.; Borenstein, J.; Vacanti, J.; Langer, R.; Karp, J. M. *Proc. Natl. Acad. Sci.* **2008**, *105*, 2307.

(4) Lee, H.; Lee, B. P.; Messersmith, P. B. *Nature* **2007**, *448*, 338.

(5) Reddy, S.; Arzt, E.; del Campo, A. *Adv. Mater.* **2007**, *19*, 3833.

(6) Ge, L.; Sethi, S.; Ci, L.; Ajayan, P. M.; Dhinojwala, A. *Proc. Natl. Acad. Sci.* **2007**, *104*, 10792.

(7) Chan, E P; Greiner, C; Arzt, E; Crosby, A J *MRS Bull.* **2007**, *32*, 496.

(8) Kim, S; Spenko, M; Trujillo, S; Heyeman, B; Santos, D; Cutosky, M R *IEEE Trans Rob.* **2008**, *24*, 65.

(9) Murphy, M P; Sitti, M *IEEE-ASME Trans. Mechatronics* **2007**, *12*, 330.

(10) Geim, A. K.; Dubonos, S. V.; Grigorieva, I. V.; Novoselov, K. S.; Zhukov, A. A.; Shapoval, S. Y. *Nat. Mater.* **2003**, *2*, 461.

(11) Sitti, M.; Fearing, R. S. *J. Adhesion Sci. Technol.* **2003**, *17*, 1055.

(12) Glassmaker, N. J.; Jagota, A.; Hui, C. Y.; Kim, J. *J. R. Soc. Int.* **2004**, *1*, 23.

(13) Greiner, C.; del Campo, A.; Arzt, E. *Langmuir* **2007**, *23*, 3495.

(14) Burton, Z.; Bhushan, B. *Nano Lett.* **2005**, *5*, 1607.

(15) Wirth, C. T.; Hofmann, S.; Robertson, J. *Diamond Relat. Mater.* **2008**, *17*, 1518.

(16) Qu, L. T.; Dai, L. M.; Stone, M.; Xia, Z. H.; Wang, Z. L. *Science* **2008**, *322*, 238.

(17) Zhao, Y.; Tong, T.; Delzeit, L.; Kashani, A.; Meyyappan, M.; Majumdar, A. *J. Vac. Sci. Technol. B* **2006**, *24*, 331.

(18) Yurdumakan, B.; Raravikar, N. R.; Ajayan, P. M.; Dhinojwala, A. *Chem. Commun.* **2005**, 3799.

(19) Jeong, H. E.; Suh, K. Y. *Nano Today* **2009**, *4*, 335.

(20) Kamperman, M.; Kroner, E.; del Campo, A.; McMeeking, R. M.; Arzt, E. *Adv. Eng. Mater.* **2010**, *12*, 335.

(21) Autumn, K. *MRS Bull.* **2007**, *32*, 473.

(22) Sameoto, D.; Menon, C. *Smart Mater. Struct.* **2010**, 19.

(23) Maeno, Y.; Ishikawa, A.; Nakayama, Y. *Appl. Phys. Exp.* **2010**, 3.

(24) Qu, L.; Dai, L. *Adv. Mater.* **2007**, *19*, 3844.

(25) Varenberg, M.; Murarash, B.; Kligerman, Y.; Gorb, S. N. *Appl. Phys. A: Mater. Sci. Process.* **2011**, *103*, 933.

(26) Kim, S.; Sitti, M. *Appl. Phys. Lett.* **2006**, *89*, 261911.

(27) Murphy, M. P.; Kim, S.; Sitti, M. *ACS Appl. Mater. Interfaces* **2009**, *1*, 849.

(28) del Campo, A.; Greiner, C.; Arzt, E. *Langmuir* **2007**, *23*, 10235.

(29) Gorb, S. N.; Sinha, M.; Peressadko, A.; Daltorio, K. A.; Quinn, R. D. *Bioinspiration Biomimetrics* **2007**, 2.

(30) Northen, M. T.; Turner, K. L. *Nanotechnology* **2005**, *16*, 1159.

(31) Qi, H. J.; Teo, K. B. K.; Lau, K. K. S.; Boyce, M. C.; Milne, W. I.; Robertson, J.; Gleason, K. K. *J. Mech. Phys. Solids* **2003**, *51*, 2213.

(32) Chung, K.-H.; Bhadriraju, K.; Spurlin, T. A.; Cook, R. F.; Plant, A. L. *Langmuir* **2010**, *26*, 3629.

(33) Oyen, M. L. *Experimental Techniques*; Wiley: New York, 2011; p 1.

(34) Ebenstein, D. M.; Pruitt, L. A. *Nano Today* **2006**, *1*, 26.

(35) Wahl, K. J.; Asif, S. A. S.; Greenwood, J. A.; Johnson, K. L. *J. Colloid Interface Sci.* **2006**, *296*, 178.

(36) Zhong, G.; Hofmann, S.; Yan, F.; Telg, H.; Warner, J. H.; Eder, D.; Thomsen, C.; Milne, W. I.; Robertson, J. *J. Phys. Chem. C* **2009**, *113*, 17321.

(37) Wirth, C. T.; Zhang, C.; Hofmann, S.; Robertson, J. *ACS Nano* **2009**, *3*, 3560.

(38) Oliver, W. C.; Pharr, G. M. *J. Mater. Res.* **1992**, *7*, 1564.

(39) Gao, Y.; Kodama, T.; Won, Y.; Dogbe, S.; Pan, L.; Goodson, K. E. *Carbon* **2012**, *50*, 3789.

(40) Gibson, L. J.; Ashby, M. .F *Cellular Solids*; Elsevier Press: New York, 1988.

(41) Johnson, K. L.; Kendall, K.; Roberts, A. D. *Proc. R. Soc. A* **1971**, *324*, 301.

(42) Tang, T.; Hui, C. Y.; Glassmaker, N. J. *J R. Soc. Interface* **2005**, *2*, 505.

(43) Jagota, A.; Bennison, S. J. *Integr. Comp. Biol.* **2002**, *42*, 1140.

(44) Jeong, H. E.; Lee, S. H.; Kim, P.; Suh, K. Y. *Colloids Surf. A* **2008**, *313*, 359.

(45) del Campo, A.; Arzt, E. *Macromol. Biosci.* **2007**, *7*, 118.

(46) Boesel, L. F.; Greiner, C.; Arzt, E.; del Campo, A. *Adv. Mater.* **2010**, *22*, 2125.

(47) Autumn, K.; Majidi, C.; Groff, R. E.; Dittmore, A.; Fearing, R. *J. Exp. Biol.* **2006**, *209*, 3558.

(48) Autumn, K.; Gravish, N. *Philos. Trans. R. Soc. A* **2008**, *366*, 1575.

(49) Demczyk, B. G.; Wang, Y. M.; Cumings, J.; Hetman, M.; Han, W.; Zettl, A.; Ritchie, R. O. *Mater. Sci. Eng., A* **2002**, *334*, 173.

(50) Li, M.; Zhao, A.; Jiang, R.; Wang, D.; Li, D.; Guo, H.; Tao, W.; Gan, Z.; Zhang, M. *Appl. Surf. Sci.* **2011**, *257*, 3336.

(51) Greiner, C.; Arzt, E.; del Campo, A. *Adv. Mater.* **2009**, *21*, 479.
(52) Schubert, B.; Lee, J.; Majidi, C.; Fearing, R. S. *J. R. Soc. Interface* **2008**, *5*, 845.